ANNUAL REVIEWS

Annual Review of Condensed Matter Physics

How Cross-Link Numbers Shape the Large-Scale Physics of Cytoskeletal Materials

Sebastian Fürthauer[1] and Michael J. Shelley[1,2]

[1]Center for Computational Biology, Flatiron Institute, New York, NY, USA; email: sfuerthauer@flatironinstitute.org, mshelley@flatironinstitute.org

[2]Courant Institute, New York University, New York, NY, USA

ANNUAL REVIEWS CONNECT

www.annualreviews.org

- Download figures
- Navigate cited references
- Keyword search
- Explore related articles
- Share via email or social media

Keywords

cytoskeleton, active matter, molecular motors, biopolymers, continuum mechanics, cell biophysics

Abstract

Cytoskeletal networks are the main actuators of cellular mechanics, and a foundational example for active matter physics. In cytoskeletal networks, motion is generated on small scales by filaments that push and pull on each other via molecular-scale motors. These local actuations give rise to large-scale stresses and motion. To understand how microscopic processes can give rise to self-organized behavior on larger scales it is important to consider what mechanisms mediate long-ranged mechanical interactions in the systems. Two scenarios have been considered in the recent literature. The first scenario is systems that are relatively sparse, in which most of the large-scale momentum transfer is mediated by the solvent in which cytoskeletal filaments are suspended. The second scenario is systems in which filaments are coupled via cross-link molecules throughout. Here, we review the differences and commonalities between the physics of these two regimes. We also survey the literature for the numbers that allow us to place a material within either of these two classes.

1. INTRODUCTION

Living systems move. On cellular scales this motion is actuated by networks of polymer filaments cross-linked by molecular-scale motors that exert forces between them. This system is collectively referred to as the cytoskeleton (1, 2). Understanding how the material properties of the cytoskeleton emerge from the properties of cytoskeletal components is one of the great challenges for soft condensed matter physics and cell biology (3). Solving it will allow biologists to predict the effects of molecular-scale perturbations on cellular organelles and enable physicists and engineers to pursue strategies for developing similarly complex and robust materials in the lab. Here, we take measure of the current state of theory for understanding the emergent physics of cytoskeletal systems based on filament-scale interactions.

Symmetry-based theories have helped clarify the fields, such as densities, velocities, and order parameters, through which the dynamics of active materials can be described on long timescales and length scales (4–6). These theories have also provided means for generating a more or less complete list of material properties (or phenomenological coefficients), such as viscosities, elastic moduli, and activity coefficients, which characterize a material. Although this type of information can be used to relate the effects of molecular perturbations to material properties (7), it does not address the question how microscale processes set the large-scale physics.

To approach this challenge, physicists and mathematicians have generalized the methods developed for polymeric and liquid crystalline systems (8, 9), and Boltzmann's statistical physics for gases, to incorporate the effects of the microscopic activity of molecular-scale motors. These efforts have led to a set of theories that describe relatively sparsely connected polymeric assemblies whose large-scale behavior is dominated by momentum transfer via solvent flows (10–12). In parallel, other groups have extended the physics of elastic networks to obtain theories for the physics of cross-linked materials on timescales that are short compared to cross-linker dynamics (13).

However, recent work has increased the awareness that many cytoskeletal systems belong to a third class of active materials. They are highly cross-linked gels, in which filaments are transiently coupled by a large number of motors and cross-links, which bind and unbind on timescales that are fast compared to the long-time, large-scale dynamics of the system. This highly cross-linked regime is set apart by new physical phenomena. Most strikingly, filaments in highly cross-linked systems can slide through the gel at speeds that are independent of the structure of their local surrounding. This phenomenon has been predicted theoretically and observed in vitro (14) and in vivo (15–17). Theories for highly cross-linked systems take inspiration from early work on actin bundles (18, 19) and describe larger networks that are cross-linked by molecular motors with different symmetries and force velocity relations (20).

The goal of this review is to give a perspective on our current understanding of the physics of cytoskeletal materials. We highlight the differences between highly and sparsely cross-linked cytoskeletal networks and their models. Where possible from published data, we classify known examples along these lines. Along the way we identify and highlight some open challenges that the field needs to address in order to enable a quantitative and predictive physics of these living materials.

In this review, we focus on continuum models and the microscopic models underlying their derivations. However, we emphasize that symmetry-based theories (21), continuum models obtained by coarse-graining microscopic models (22, 23), and agent-based models for the same systems (24–27) have been extensively studied in numerical simulations as well.

In Section 2, we review the key constituents of cytoskeletal materials. Then, in Section 3, we propose a classification of cytoskeletal structures as either highly or sparsely cross-linked. To guide us in this, we review the conditions under which a material's long-range momentum transport is dominated by cross-link interactions or by solvent flow, respectively. We then classify studied

cytoskeletal materials given published data. After that, in Section 4, we review the theoretical descriptions of both highly and sparsely cross-linked materials, highlighting and contrasting their different physics. We point out how these differences can be used as both predictive and diagnostic tools.

2. KEY CONSTITUENTS OF THE CYTOSKELETAL NETWORKS

The cytoskeleton is the cellular machinery that enables cells to do mechanical work on their organelles and on their surroundings. The cytoskeleton consists of polymer filaments, proteins that cross-link and actuate these filaments, and regulators that help organize and coordinate their functions in time and space. All of these constituents are suspended in cytoplasm, which is the aqueous slurry that makes up a cell's interior.

2.1. Cytoskeletal Filaments

Several types of cytoskeletal filaments exist. The two most studied and most abundant ones are filamentous actin and microtubules (2; see **Figure 1**). Both are structurally polar, meaning that their molecular structure differentiates one direction from the other. They are both transient because they are constantly assembling and disassembling. They are active because filament assembly and disassembly are driven by energy derived from GTP (guanosine triphosphate). Though it is sufficient to think of cytoskeletal filaments as polar rods for our purposes here, we want to emphasize that in typical in vivo systems the lifetime of actin filaments and microtubules is often much shorter than the timescale of large-scale rearrangements of the system. One typical example is gastrulation in fruit fly. This process takes about 2 h and is driven by actomyosin, which
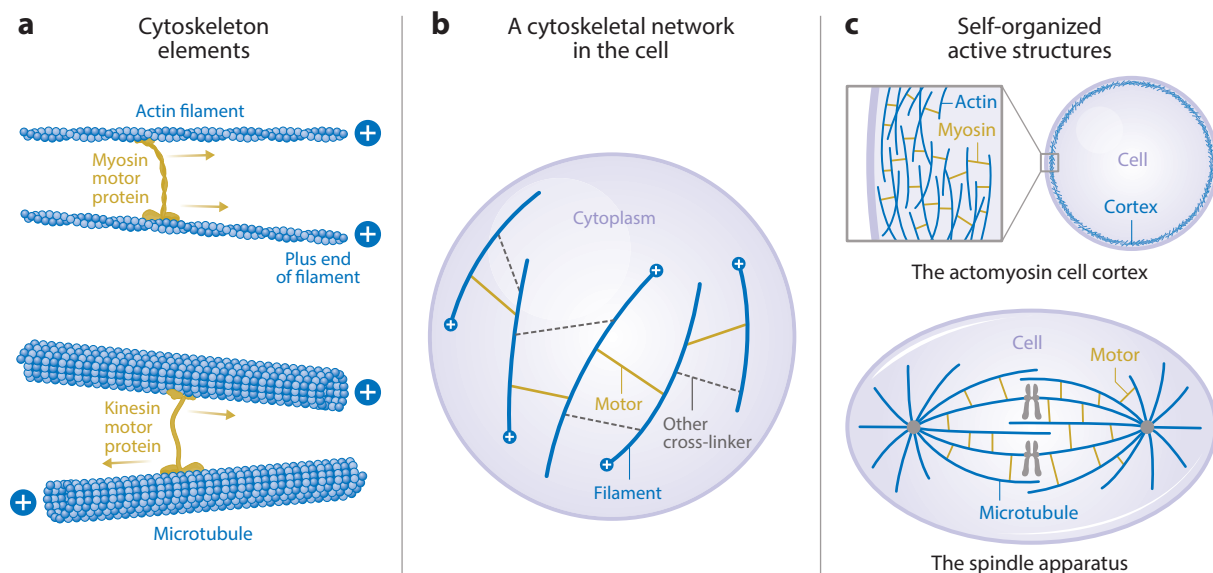

Figure 1

(*a*) Polar cytoskeletal filaments are coupled and actuated by molecular-scale motors. Collectively they form the cytoskeletal networks (*b*), which are the materials that make up many important biological structures (*c*). Note that the molecular motors represented here should be read as abstractions for possibly very complex molecular structures. For instance myosin motors collectively form minifilaments, dyneins act in concert with adaptor proteins, and kinesins often dimerize.

turns over within minutes (28). Another such process is the separation of chromosomes during cell division in the nematode worm *Caenorhabditis elegans*, which takes tens of minutes and is achieved by microtubules that have lifetimes of tens of seconds (29). There are additional cytoskeletal filaments beyond actin and microtubules; they are largely called intermediate filaments. Examples include keratins, which are a large family of proteins that encompass vimentins (which play a role in cell motility) and lamins (which act as a mechanical scaffolding for the cell nucleus). These intermediate filaments—so-called because their thickness in the electron tomographs in which they were first characterized was between that of thin actin filaments and that of thick myosin minifilaments—are typically longer-lived, apolar, and hypothesized to provide cells with long time elasticity. Kinesins, myosins, and dyneins that link intermediate filaments to the microtubule and actin cytoskeleton have been identified, but so far their role remains underexplored.

2.2. Active and Passive Cross-Linkers

The second class of molecules that are important for the cytoskeleton are cross-linking proteins, which connect cytoskeletal filaments to each other and to other structures such as chromosomes and membranes. Too many types exist to do them justice in a review focused on the physics of the cytoskeleton, so we refer the reader to References 30 and 31 for recent perspectives on actin and microtubule associated cross-linkers. Many of these cross-linkers are molecular-scale motors. This means they have access to a chemical fuel reservoir—in general adenosine triphosphate (ATP)—from which they can draw power to do mechanical work upon the structures they cross-link. Motors can walk along cytoskeletal filaments, acting as moving cross-links, which slides filaments past each other. Or, they can carry a cargo, like a vesicle or a mitochondrion, along filaments. The most abundant actin-associated molecular motors are myosins. The most abundant microtubule-associated ones are dyneins and kinesins. Typically motors can exert forces of up to several pico-Newtons, and their unloaded walking speeds on filaments can vary from nanometers to microns per second. Finally, motors can be more or less processive. A motor's processivity measures the expected number of steps a motor typically takes before it unbinds from the filament to which it is attached (1, 2).

2.3. Cytoplasm

The last important actor in understanding the physics of the cytoskeleton is the aqueous slurry in which it is immersed. Although the rheology of the cytoplasm is most certainly complex (32), most current physical theories for the cytoskeleton ignore this fact—mainly because the detailed characteristics of cytoplasmic rheology are poorly understood and difficult to model. The theories that we review thus approximate it as a very viscous Newtonian fluid with a viscosity between 100 and 1,000 times that of water (see, for example, 33).

2.4. Forces and Torques in Cytoskeletal Networks

The goal of a physical theory for the cytoskeleton is to predict how filaments in a cytoskeletal network rearrange in response to the forces that they experience and produce. The larger goal is a quantitative understanding of the mechanical processes that allow cytoskeletal structures to self-organize and perform their complex tasks within cells.

The elementary starting point is characterizing the total force $\mathbf{F}_i$ that acts on the ith filament in the network. We assume that it has the form

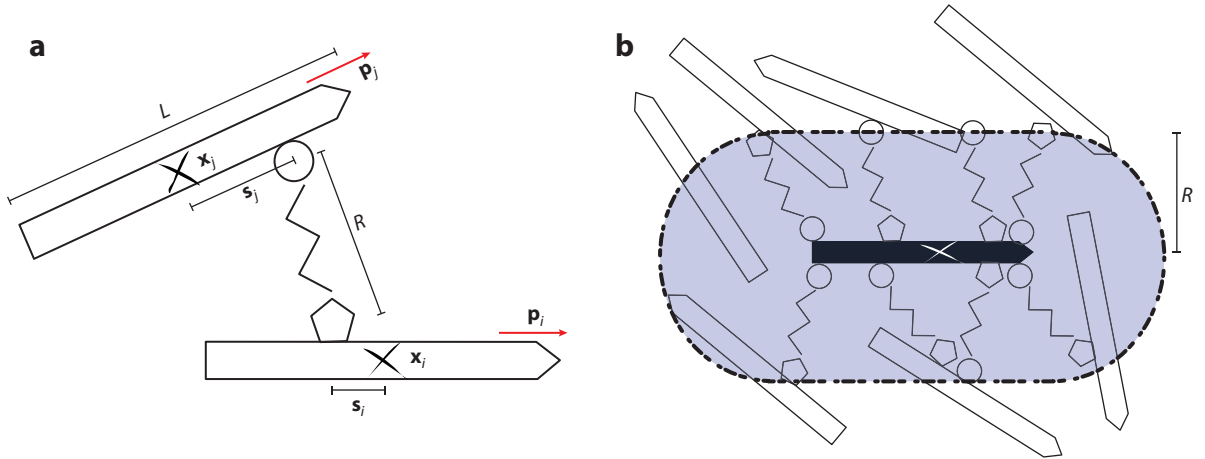$$\mathbf{F}_i = \sum_j \mathbf{F}_{ij}^{\times} + \mathbf{F}_i^{s} = 0, \qquad\qquad 1.$$

Figure 2

(*a*) Interaction between two cytoskeletal filaments i and j via a molecular motor. Filaments are characterized by their positions, $\mathbf{x}_i$ and $\mathbf{x}_j$, and orientations, $\mathbf{p}_i$ and $\mathbf{p}_j$. A motor connects a position s_i on microtubule i with position s_j on microtubule j. A motor consists of two heads that can be different (*circle* or *pentagon*) and are connected by a linker (*black zig-zag*) of length R. (*b*) The total force on filament i is given by the sum of the forces exerted by all heads that connect the filament into the network. The shaded area shows all geometrically accessible positions that can be cross-linked to the central (*black*) filament. Figure adapted from Reference 20 with permission.

which vanishes because cytoskeletal systems are overdamped (see **Figure 1*b***). The total force on each filament consists of cross-link mediated forces $\sum_j \mathbf{F}_{ij}^{\times}$ and a contribution $\mathbf{F}_i^s$, which comes from the drag between filaments and a moving solvent. The cross-link-mediated force between filaments i and j is given by

$$\mathbf{F}_{ij}^{\times} = \int_{-L/2}^{L/2} \mathrm{d}s_i \int_{-L/2}^{L/2} \mathrm{d}s_j \int_{\Omega(\mathbf{x}_i + s_i \mathbf{p}_i)} \mathrm{d}^3 x\, \delta(\mathbf{x} - \mathbf{x}_j - s_j \mathbf{p}_j) \mathbf{f}_{ij}, \qquad 2.$$

where $\mathbf{f}_{ij}$ is the force density exerted by cross-linkers between the arclength positions s_i and s_j on the two filaments i and j, respectively (see **Figure 2**). Here, $\Omega(\mathbf{x})$ is a sphere centered around the point $\mathbf{x}$ and whose radius R is the size (maximal extension) of the cross-linker. Here, all filaments are taken to be rigid and to have the same length L. Analogous expressions for the torques and total torque on filament i hold.

In the following, we argue that modeling of cytoskeletal networks has focused on two different regimes: (*a*) a highly cross-linked regime in which the long-range momentum transport through the gel is dominated by cross-linking forces and (*b*) a regime in which momentum transport through the solvent dominates. Theories for the two limits make very different predictions for the scaling of important material properties and dynamics.

3. WHICH CYTOSKELETAL MATERIALS ARE HIGHLY CROSS-LINKED?

We now discuss the crossover between the highly and sparsely cross-linked regimes and try to classify a few well-studied cytoskeletal systems along these lines. For this, we define the density of cytoskeletal filaments $\rho = \sum_i \delta(\mathbf{x}_i - \mathbf{x})$ and the force density $\mathbf{f} = \sum_i \delta(\mathbf{x}_i - \mathbf{x})\mathbf{F}_i$. Because cross-link-mediated interactions are short ranged we can write the cross-link-mediated forces in terms of a stress tensor, $\mathbf{\Sigma}$:

$$\mathbf{f} = \nabla \cdot \mathbf{\Sigma} - \Gamma \rho(\mathbf{v} - \mathbf{v}^s) + \mathcal{O}\left(L^4\right) = 0, \qquad 3.$$

where L is assumed small compared to the system scale (20), and we have included a drag term for momentum exchange with the solvent. In the following, we use the word gel to signify the filaments and cross-links and solvent for the cytoplasm in which they are immersed. The gel stress $\boldsymbol{\Sigma}$ encodes the momentum flux through the cross-links that connect filaments, and $\Gamma\rho$ is the friction coefficient between the gel and the solvent. Finally, $\mathbf{v}$ and $\mathbf{v}^s$ are the gel and solvent center of mass velocities, respectively. If we take the solvent to be a Newtonian fluid with viscosity μ, it obeys the Stokes equation,

$$\mu\Delta\mathbf{v}^s - \nabla\boldsymbol{\Pi}^s + \Gamma\rho(\mathbf{v} - \mathbf{v}^s) = 0, \qquad\qquad 4.$$

where $\boldsymbol{\Pi}^s$ is the hydrostatic pressure. The characteristic length scale over which momentum is transported through the solvent, the permeation length, is thus given by

$$\ell^s = \sqrt{\frac{\mu}{\rho\Gamma}}, \qquad\qquad 5.$$

which decreases as the density ρ of filaments in the gel increases. Conversely, cross-links generate friction between the filaments they connect, which leads to a viscous contribution $\mu^g\rho^2\nabla\mathbf{v}$ to $\boldsymbol{\Sigma}$, i.e., proportional to the strain rate of the gel and to the number of filament–filament interactions mediated by cross-links (14, 20). Here, $\mu^g\rho^2$ is the gel viscosity. Thus, we expect the typical length scale over which momentum is transported through the gel to be

$$\ell^g = \sqrt{\frac{\mu^g\rho^2}{\Gamma\rho}}, \qquad\qquad 6.$$

which increases with filament density. Note that the dimensions of μ and μ^g are different. Whereas μ has dimensions of viscosity, μ^g has dimensions of viscosity per square density. The implied assumption of this calculation is that the number of realized cross-link connections is limited by the number of geometrically possible filament–filament interactions and not the number of cross-linking molecules available. However, it can easily be generalized.

In the following, we consider a system highly cross-linked if $\ell^g \gg \ell^s$ and sparsely cross-linked if $\ell^s \gg \ell^g$. We next review the literature and overview which cytoskeletal systems are highly or sparsely cross-linked, respectively (see **Figure 3**).

a Sparsely cross-linked network   **b** Highly cross-linked network

Plus end of filament

Cross-link (motor)
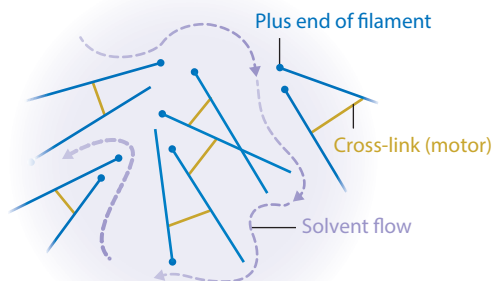
Solvent flow

Long-range dynamics
determined by solvent flow
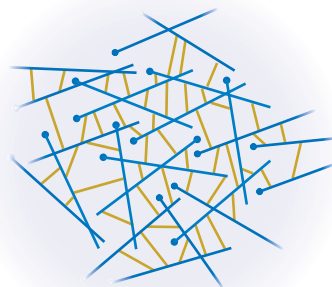
Long-range dynamics
determined by active cross-links

Figure 3

Illustration of the key differences between (*a*) sparsely and (*b*) highly cross-linked networks, emphasizing the dominant mechanisms of large-scale momentum transport.

3.1. The Cell Cortex

The cell cortex is a thin layer of actin filaments that localize at the cell membrane (see **Figure 4***a*). It is actuated by nonmuscle myosin 2 and held together by a variety of cross-linkers and proteins, which regulate assembly and disassembly of both thick (myosin) filaments and thin (actin) filaments (30). Typically the thickness of the cortical layer is 300–1,000 nm (34). Flow of actomyosin is vital for cell polarity establishment (the process by which cells break the symmetry between two daughter cells; 35, 36), cell migration and shape changes (37), and cell division (38), as well as regulating cellular surface tension (39). On timescales longer than filament lifetimes, the cell cortex is well described as an active fluidic material (7, 35, 40).

Comprehensive estimates of the numbers of cross-links in the actin cell cortex are hard to come by. That said, many actin filaments are nucleated by the nucleator Arp2/3 which is a cross-linker itself. In Reference 43, the authors estimate that roughly nine out of ten actin filaments are nucleated by Arp2/3, whereas about one out of ten is nucleated by formins. This finding suggests that the actin cortex is highly cross-linked starting from its nucleation. Furthermore, actin filaments are actively cross-linked by myosin motors and other cross-linkers. In Reference 44, the authors count the numbers of the most important actin binding partners in fission yeast cells. They find that the number of cross-linkers and motors acting on actin filaments is comparable to (or larger than) the number of nucleators (Arp2/3 and formins) in the system. Thus, if one estimates that the number of filaments is roughly proportional to the number of available nucleators, one concludes that several cross-linking interactions per filament exist at any given time. That is, the actin cortex is highly cross-linked.
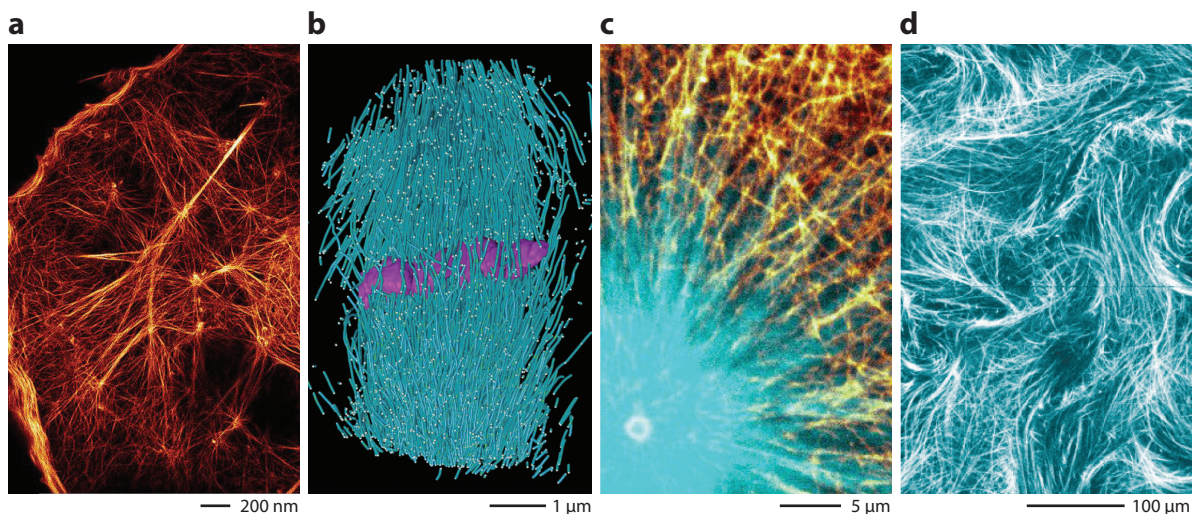

Figure 4

Biological and artificial cytoskeletal networks: (*a*) SIM-TIRF superresolution microscopy image of the actin cortex from a kidney culture cell. (*b*) Electron tomography reconstruction of the inner spindle microtubules of an embryonic *Caenorhabditis elegans* mitotic spindle. (*c*) Spinning disk fluorescence microscopy image of microtubules and actin in a *Xenopus laevis* interphase aster in egg extract. Image courtesy of James Pelletier. (*d*) Snapshot from an experiment on an active microtubule nematic synthesized from engineered multimeric kinesin-1 motors and stabilized microtubules. Throughout the figure, actin filaments are represented in orange and microtubules in blue. Panel *a* adapted with permission from Reference 41; panel *b* adapted from Reference 29; and panel *d* adapted with permission from Reference 42.

3.2. The Spindle

The spindle is the cellular apparatus that segregates chromosomes during cell division. Its main constituents are microtubules, which are cross-linked and actuated by dynein and kinesin molecular motors (see **Figure 4b**). Despite having common constituents and function, spindle structure can vary widely, even in a single organism.

One spindle whose physics has been studied extensively is the meiotic spindle of *Xenopus laevis*. This spindle can be reconstituted in frog egg extract, which makes it particularly attractive to study ex vivo. These spindles are large—about 50 μm long—and consist of microtubules whose lengths and lifetimes are exponentially distributed around an average length and lifetime of about 6 μm and 20 s, respectively (45). They have been shown to obey the fluctuation spectra expected for active nematic gels (46). In these spindles, microtubules nucleate by an autocatalytic mechanism in which preexisting microtubules recruit growth factors that initiate the formation of new microtubules (47–51). This mechanism implies that filaments are created cross-linked to the spindle gel. The details of the pathway controlling nucleation have been investigated (52, 53). The motor proteins dynein and Eg-5 kinesin cross-link the spindle network further. Although direct measurements of the number of Eg-5 kinesin cross-links are not available, observations of microtubule motion in spindles allow an estimate. In Reference 17, the authors quantify the motion and polarity of microtubules in *Xenopus* spindles. They estimate that two or more motors per filament are required to explain experimental observations that velocity fluctuations are highly correlated throughout the whole spindle. In our language, this means that ℓ^g is comparable with system size and, thus, that the *Xenopus* spindle is highly cross-linked.

Another well-studied spindle is the embryonic mitotic spindle of the nematode worm *C. elegans*. These spindles are much smaller—10 μm pole to pole—and have been fully reconstructed using electron tomography (29; see **Figure 4c**). Using this structural information, together with light microscopy and mathematical modeling, the authors in Reference 54 argue that the connection between spindle poles and chromosomes is indirectly maintained by microtubules cross-linking to other microtubules. Although the evidence is indirect, it is suggestive of a highly cross-linked network.

The third example that we want to highlight here is the female meiotic spindle, also in *C. elegans*. This spindle is about half the size of the mitotic one and has also been reconstructed in tomography. The findings from tomography studies (55, 56) suggest that it consists of short and short-lived microtubules and is structurally quite similar to the *X. laevis* meiotic spindle. It is thus tempting to speculate that this spindle too is a highly cross-linked network.

3.3. Microtubule Asters

In cells, spindles are positioned for cell division by microtubule asters, which emanate from the spindle poles and grow out toward the cortex (see **Figure 4c**). In smaller cells, microtubules interacting with cortex are important for spindle positioning (33, 57, 58). Recent work in *C. elegans* embryos suggests that dynein-mediated pulling forces from cortically bound dynein are crucial (59).

In larger cells, such as the *Xenopus* zygote, the situation is somewhat more complicated, because cytoskeletal filaments are in general much shorter than the typical cell radii (60). Thus it has been proposed that in these cells spindles are positioned by cytoplasmic pulling, that is, by dynein motors, which carry a cargo from the aster periphery toward its center. This would cause an active drag against the cytoplasmic fluid, which would ultimately cause spindle centering (61, 62). To test this hypothesis the authors of Reference 63 coimaged the cytoskeletal actin, microtubules, and membranous networks. They find that these networks move against each other near aster boundaries, but move together near the aster's center. It is thus tempting to ask what explains

these different behaviors. One appealing hypothesis is that these asters are highly cross-linked near their centers, and less cross-linked near aster cores.

3.4. Artificial Systems

Given the complexity and the sheer number of different constituents of cytoskeletal networks in living cells, biophysicists have developed simplified in vitro systems made from cytoskeletal components (see **Figure 4c**). Here, the physics of cytoskeletal networks can be studied at a reduced complexity and in a more controllable environment. Beyond that, they have provided foundational examples of out-of-equilibrium materials.

One prominent system discussed in Reference 64 is made from stable microtubules and kinesin-1 motors joined by engineered linkers. This same mixture has been used to study active materials in bulk and on two-dimensional interfaces (64), and in vesicles (65), rigid confinements (66, 67) and droplets (68). The same system has also been adapted to study disclination loops in three-dimensional active nematics (69). It is surprising, given the importance of these systems, that the structure and number of cross-links that bind microtubules remain relatively unexplored. More studies are needed to solidly classify these particular systems as either highly or sparsely cross-linked.

Somewhat more recently, actin-based active networks have been synthesized. Many of the key findings of this line of research is summarized in Reference 70. These systems are in general driven by the molecular motor myosin and require the admixture of passive cross-linkers to generate active contractions. This peculiarity has been attributed to a liquid–gel transition, which may imply that the contractile states of these actomyosin networks are in the highly cross-linked regime.

There is a growing list of in vitro systems using different motors and filaments assembled in cell extract or fully reconstituted such as those in References 71 and 72 or the ones reviewed in References 70 and 73. For most of these systems, it remains unclear where they fall on the range from sparsely to highly connected systems.

4. THEORETICAL DESCRIPTIONS OF CYTOSKELETAL SYSTEMS

Much of our current theoretical understanding of cytoskeletal active matter derives from the remarkable success of extending the broken-symmetry hydrodynamic theory for liquid crystals (9) to active materials in which microscale nonequilibrium processes can generate force and torque dipoles (4–6). These theories have clarified the fields (densities, velocities, order parameters, etc.) through which to describe the dynamics of a cytoskeletal material on long-wave hydrodynamic scales (see **Figure 5**), and which material properties, such as the viscosities and activity coefficients, are needed to characterize these materials. More microscopic theories derive the values of material properties and their microscopic origins.

We start by reviewing the fields and material properties that we use to characterize cytoskeletal materials. We then review theoretical predictions for how these material properties are determined in highly and sparsely cross-linked networks.

4.1. Hydrodynamic Variables

We seek to describe the evolution of a cytoskeletal system with a small number of continuous fields. At large timescales and length scales, the fields needed to sufficiently characterize a material are those associated with conserved quantities and those associated to continuous broken symmetries (74; see **Figure 5a**). We first introduce the fields associated with conserved quantities.
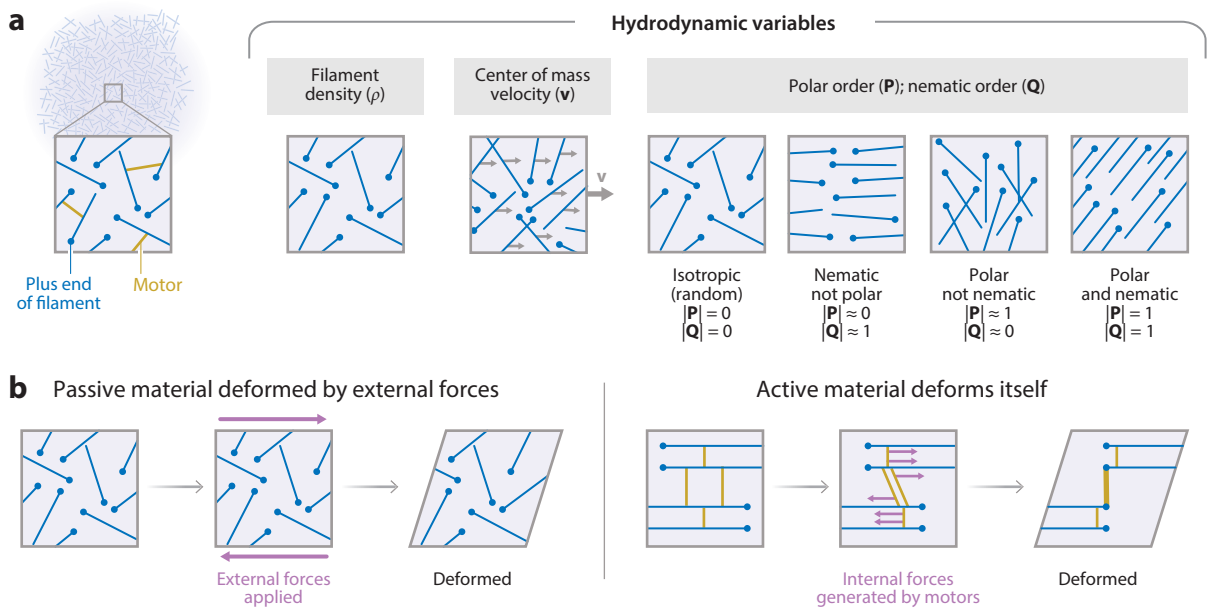
Figure 5

(*a*) Illustration of the important hydrodynamic variables. (*b*) Illustration of externally strained and self-strained materials.

The first is the total mass density $\rho^{\text{tot}}(\mathbf{x}, t)$ of the material. Because mass can be neither created nor destroyed,

$$\partial_t \rho^{\text{tot}} = -\nabla \cdot \mathbf{g}^{\text{tot}}, \qquad 7.$$

where $\mathbf{g}^{\text{tot}}(\mathbf{x}, t)$ denotes the total mass flux, which is also referred to as momentum density. In the cytoskeletal systems of interest here, the total mass density consists of solvent and gel contributions, such that $\rho^{\text{tot}} = \rho + \rho^{\text{s}}$, where ρ is the gel contribution, by which we mean the mass of filaments and proteins attached to filaments. In general, chemical processes, such as filament nucleation and polymerization and the binding and unbinding of proteins, can convert solvent mass into gel mass and vice versa. Thus, we can write

$$\partial_t \rho = -\nabla \cdot \rho \mathbf{v} + R, \qquad 8.$$

$$\partial_t \rho^{\text{s}} = -\nabla \cdot \rho^{\text{s}} \mathbf{v}^{\text{s}} - R, \qquad 9.$$

where R is the mass conversion rate from chemical reactions, and we have defined the gel and solvent velocities by $\mathbf{g}^{\text{tot}} = \rho \mathbf{v} + \rho^{\text{s}} \mathbf{v}^{\text{s}}$. In living materials, the dominant contribution to R is filament polymerization and depolymerization, which in general is highly regulated. For instance, in *Xenopus*'s meiotic spindles the dominant mode of filament creation is autocatalytic, and new filaments nucleate in a branching process from preexisting ones (47–53).

The second field that arises from conservation considerations is the momentum density itself. In the absence of external forces, the momentum density $\mathbf{g}^{\text{tot}}(\mathbf{x}, t)$ can only change by a momentum flux,

$$\partial_t \mathbf{g}^{\text{tot}} = \nabla \cdot \mathbf{\Sigma}^{\text{tot}}, \qquad 10.$$

where $\boldsymbol{\Sigma}^{\mathrm{tot}}(\mathbf{x}, t)$ is total stress in the material. Like the mass flux, we can write $\boldsymbol{\Sigma}^{\mathrm{tot}} = \boldsymbol{\Sigma} + \boldsymbol{\Sigma}^s$ and force balance equations for the gel and solvent components of the material separately. Under the assumptions that the solvent is Newtonian, that inertial terms can be neglected, and that the force exerted between the gel and fluid phases is linear in the gel density and their velocity difference, one recovers Equations 3 and 4. Thus, the fields that we need to keep track of, because they are associated to conserved quantities, are $\rho, \rho^s, \mathbf{v}$, and $\mathbf{v}^s$. We next introduce the fields that are associated with continuous broken symmetries.

Order parameter fields characterize the conformational state of the material. For our purposes here, we assume that cytoskeletal filaments are rod-like and rigid. Then the tensor orientation order parameter $\mathcal{Q}(\mathbf{x}, t)$ naturally arises. The scalar orientation order parameter and director field devolve from $\mathcal{Q}$. Unlike purely nematic systems, cytoskeletal filaments like microtubules or actin are polar, as are the motor-mediated forces acting upon them. Hence, we also need a polar order parameter $\mathbf{P}(\mathbf{x}, t)$. If the system were characterized at the microscopic level by a particle distribution function $\psi(\mathbf{x}, \mathbf{p}, t)$ (8) with $\mathbf{p}$ being the particle orientation vector on the two-sphere, then these order parameters arise as its $\mathbf{p}$-moments, $\mathbf{P} = \langle \mathbf{p} \rangle / \rho$ and $\mathcal{Q} = \langle \mathbf{pp} \rangle / \rho$, where the angular brackets denote a distributional averaging over the $\mathbf{p}$-sphere.

We emphasize that $\mathbf{P}$ and $\mathcal{Q}$ are independent fields, and a complete description of cytoskeletal networks is needed to keep track of both. To understand this, consider two filaments coupled by a motor protein with two heads, with each attached to one of the filaments and walking toward a plus-end. If such a motor were to couple two antialigned filaments, it would induce relative sliding. However, if it coupled two aligned filaments, then the filaments would not move. As a consequence, on large scales the material properties of cytoskeletal networks can depend on $\mathbf{P}$ and $\mathcal{Q}$ in different ways, and in particular the active stresses generated by molecular motors will often be different between polar and nematic regions in the same system. This is clear in the particular theories we discuss below. In general, higher-order symmetry fields exist, but we ignore them here for simplicity.

In summary, we seek to describe the cytoskeletal systems in terms of just a few coarse-grained continuous fields. They are the densities ρ and ρ^s, the velocity fields $\mathbf{v}$ and $\mathbf{v}^s$, and the order parameter fields $\mathcal{Q}$ and $\mathbf{P}$. Thus, the next task is to arrive at expression for the stresses $\boldsymbol{\Sigma}^{\mathrm{tot}}$ and $\boldsymbol{\Sigma}$, the transport operators for the order parameter fields $\mathcal{Q}$ and $\mathbf{P}$, and the chemical reaction rate R, in terms of hydrodynamic variables. In this review, we are concerned with the expressions for the stresses first and foremost.

4.2. Material Properties of Active Cytoskeletal Networks

Given the set of hydrodynamic variables, symmetry-based theories postulate material laws for all unknown quantities by writing down all symmetry-allowed terms that respect the invariances of the systems, such as translation and rotation invariance. How to obtain symmetry-based material equations from symmetry considerations or from nonequilibrium thermodynamics considerations is reviewed elsewhere in great detail (6, 21).

For our purposes here, it is sufficient to express the total stress by the equation

$$\boldsymbol{\Sigma}^{\mathrm{tot}} = \chi^v : \nabla \mathbf{v} + \chi^s : \nabla \mathbf{v}^s + \chi^a : \nabla \mathbf{P} + \Pi^a \mathcal{I} + \mathcal{A}^{(\mathbf{P})} \mathbf{PP} - \mathcal{A}^{(\mathcal{Q})} \mathcal{Q} + \bar{\boldsymbol{\Sigma}}, \qquad 11.$$

which obeys the symmetry constraints discussed in References 21 and 6. Here, χ^v is the fourth-rank gel viscosity tensor, χ^s is a fourth-rank solvent viscosity tensor, and χ^a is a fourth-rank tensor that quantifies active polar stresses proportional to gradients in gel polarity $\mathbf{P}$. The coefficients $\mathcal{A}^{(\mathbf{P})}$ and $\mathcal{A}^{(\mathcal{Q})}$ quantify the magnitude of active polar and active nematic stresses in the material, respectively. Furthermore, Π^a acts as an active pressure and $\bar{\boldsymbol{\Sigma}}$ denotes other stresses in the system,

which stem from hydrostatic and steric exclusion and alignment effects. For an in-depth discussion see References 9 and 6. Together, χ^v, χ^a, χ^s, Π^a, $\mathcal{A}^{(\mathbf{P})}$, and $\mathcal{A}^{(\mathcal{Q})}$ are the material properties of the cytoskeletal filament network. They in turn depend on the state of the network, that is, the hydrodynamic variables, and need to be either measured in an experiment or derived from microscopic considerations to allow a complete description of the material. Symmetry-based theories also elucidate the form of the transport equations for $\mathbf{P}$ and $\mathcal{Q}$. We refer to References 6 and 21 for a more complete discussion.

In this review, we are concerned with theories that derive expressions for the phenomenological coefficients in Equation 11 from microscale considerations of motors and filaments. In particular, we want to contrast theories for highly cross-linked and sparsely cross-linked systems. We highlight that the functional dependencies of χ^v, χ^a, χ^s, Π^a, $\mathcal{A}^{(\mathbf{P})}$, and $\mathcal{A}^{(\mathcal{Q})}$ change between these two regimes.

4.3. The Highly Cross-Linked Regime of Cytoskeletal Networks

We first review theories for the hydrodynamic limit of the highly cross-linked regime of cytoskeletal networks. We consider a cytoskeletal material to be highly cross-linked if $\ell^g \gg \ell^s$. The hydrodynamic limit of such a material is dominated by cross-link interactions, and thus solvent-mediated interactions can be ignored because the length scale of momentum transport associated with $\boldsymbol{\Sigma}$ is much larger than that associated with $\boldsymbol{\Sigma}^s$ (see **Figure 3**). Thus, these theories assume that $\boldsymbol{\Sigma}^{\text{tot}} = \boldsymbol{\Sigma}$, which implies $\mathbf{v}^s = \mathbf{v}$ and that $\boldsymbol{\Sigma}^s$ is negligible.

To our knowledge, this limit of active gels was first discussed in the context of studying actin bundles (19, 75), where the authors proposed a one-dimensional model for describing actin structures in the cortex. Only recently have these ideas been extended to larger three-dimensional systems. In References 14 and 20, a phenomenological model for the force density $\mathbf{f}_{ij}$, generated by cross-links between filaments, was proposed. In this model, the force density is given by

$$
\begin{aligned}
\mathbf{f}_{ij} = {} & K(s_i, s_j)\left(\mathbf{x}_i + s_i\mathbf{p}_i - \mathbf{x}_j - s_j\mathbf{p}_j\right) \\
& + \gamma(s_i, s_j)\left(\mathbf{v}_i + s_i\dot{\mathbf{p}}_i - \mathbf{v}_j - s_j\dot{\mathbf{p}}_j\right) \\
& + \left[\sigma(s_i, s_j)\mathbf{p}_i - \sigma(s_j, s_i)\mathbf{p}_j\right].
\end{aligned}
\tag{12.}
$$

The functions $K(s_i, s_j)$, $\gamma(s_i, s_j)$, and $\sigma(s_i, s_j)$ characterize the types of forces exerted by cross-link populations between the arclength positions s_i and s_j on filaments i and j. The coefficient K captures effects of cross-link elasticity, the coefficient γ acts as an effective frictional coupling between filaments, and σ characterizes the active forcing from motor stepping (see **Figure 2**). The main conceptual advance between this phenomenological model and the ones proposed in earlier work is that here $\mathbf{f}_{ij}$ explicitly depends on the velocities and rates of rotation of filaments i and j. With this dependence, in a dense system the dynamics of all filaments in the system become tightly coupled. In contrast, earlier work (11, 18, 23, 76) had posited motor interactions that depend only on the relative orientations and center of mass positions of filaments, effectively constraining themselves to pairwise interactions.

From Equation 12, one calculates the stress in the network using

$$
\boldsymbol{\Sigma} = -\frac{1}{2}\sum_{i,j}\left[\begin{array}{c} \delta(\mathbf{x} - \mathbf{x}_i)\delta(\mathbf{x}' - \mathbf{x}_j) \\ \left(\mathbf{x}_i - \mathbf{x}_j + s_i\mathbf{p}_i - s_j\mathbf{p}_j\right)\mathbf{f}_{ij} \end{array}\right]^{ij}_{\Omega(\mathbf{x}_i)},
\tag{13.}
$$

where the brackets $\lfloor \cdots \rceil^{ij}_{\Omega(\mathbf{x}_i)}$ denote the coarse-graining operation

$$\lfloor \phi \rceil^{ij}_{\Omega(\mathbf{x}_i)} = \int\limits_{-\frac{L}{2}}^{\frac{L}{2}} ds_i \int\limits_{-\frac{L}{2}}^{\frac{L}{2}} ds_j \int\limits_{\Omega(\mathbf{x}_i)} d\mathbf{x}^3 \phi. \qquad 14.$$

Here, $\Omega(\mathbf{x})$ is a sphere centered around the point $\mathbf{x}$, whose radius R is the size (maximal extension) of the cross-linker. In this version of the theory, all filaments are taken to have the same length L. Thus, the operation $\lfloor \cdots \rceil^{ij}_{\Omega(\mathbf{x}_i + s_i \mathbf{p}_i)}$ integrates its argument over all geometrically possible cross-link-induced interactions.

The emergent material properties turn out to depend on a small set of s-moments of the phenomenological coefficients K, γ, and σ. These moments are given by

$$X_{nm}(\mathbf{x}) = \lfloor X(s_i, s_j) s_i^n s_j^m \rceil^{ij}_{\Omega(\mathbf{x})}, \qquad 15.$$

where X can be K, γ, or σ. More explicitly,

$$K_0 = K_{00} = \lfloor K(s_i, s_j) \rceil^{ij}_{\Omega(\mathbf{x}_i)}, \qquad 16.$$

$$K_1 = K_{10} = K_{01} = \lfloor s_i K(s_i, s_j) \rceil^{ij}_{\Omega(\mathbf{x}_i)}, \qquad 17.$$

$$\gamma_0 = \gamma_{00} = \lfloor \gamma(s_i, s_j) \rceil^{ij}_{\Omega(\mathbf{x}_i)}, \qquad 18.$$

$$\gamma_1 = \gamma_{10} = \gamma_{01} = \lfloor s_i \gamma(s_i, s_j) \rceil^{ij}_{\Omega(\mathbf{x}_i)}, \qquad 19.$$

$$\sigma_0 = \sigma_{00} = \lfloor \sigma(s_i, s_j) \rceil^{ij}_{\Omega(\mathbf{x}_i)}, \qquad 20.$$

$$\sigma_{10} = \lfloor s_i \sigma(s_i, s_j) \rceil^{ij}_{\Omega(\mathbf{x}_i)}, \qquad 21.$$

$$\sigma_{01} = \lfloor s_j \sigma(s_i, s_j) \rceil^{ij}_{\Omega(\mathbf{x}_i)}. \qquad 22.$$

The coefficients K_0, γ_0, and σ_0 quantify the net elastic, friction, and motor force, respectively, that cross-links exert between two filaments. The coefficients γ_1, σ_{10}, and σ_{01} quantify how nonuniformity in friction and motor forces effect the coupling between filaments. For instance, the friction anisotropy is positive, $\gamma_1 > 0$, if most of the friction is exerted near the end of the filament that the motor walks toward. Similarly, σ_{01} and σ_{10} are positive if most of the motor force is exerted toward the end that the motor walks toward. In practice, all these coefficients can depend in complex ways on filament geometries and the biochemical environment of the system. Detailed experiments are needed to infer the values of these coefficients in specific contexts and understand the mechanisms that set them on microscopic scales.

With these definitions, and dropping explicit cross-link-mediated torques such as the ones that would emerge if cross-links also acted as torsional springs, the authors of Reference 20 find for the viscosity tensor

$$\chi^v_{\alpha\beta\gamma\mu} = \rho^2 \gamma_0 \left[\frac{3R^2}{10} \delta_{\alpha\gamma} \delta_{\beta\mu} + \frac{L^2}{12} \gamma_0 \left(Q_{\alpha\gamma} \delta_{\beta\mu} - Q_{\alpha\beta} Q_{\gamma\mu} \right) \right], \qquad 23.$$

and, very importantly, that

$$\chi^a_{\alpha\beta\gamma\mu} = \frac{\sigma_0}{\gamma_0} \chi^v_{\alpha\beta\gamma\mu} \qquad 24.$$

for the coefficient quantifying the active polar stress.

The relation between Equations 23 and 24 implies that we can combine the first two terms of Equation 11 into

$$\mathbf{\Sigma}^{ss} = \chi^v : \left(\nabla \mathbf{v} + \frac{\sigma_0}{\gamma_0} \nabla \mathbf{P} \right),$$
25.

which we call the self-straining stress. In this type of material, σ_0/γ_0 is essentially the free velocity of the motors and cross-links coupling filaments. Thus, the state of zero self-straining stress is one in which the viscous stress exactly balances the active polar stress, which can be achieved when all filaments in the material move at the motor speed in the direction in which they point (14). This self-straining state is a consequence of the fact that the same active cross-links that drive filament motion also couple the dynamics over long length scales. In essence, in a material in which the cross-linking is provided by active cross-links, filaments can move through the material at the preferred speed of the motor without stressing the material (see **Figure 5**).

The same calculation also makes predictions for other active stresses in the material (20). One finds

$$A^{(Q)} = \rho^2 \left(\sigma_{10} - \sigma_0 \frac{\gamma_1}{\gamma_0} + \frac{L^2}{12} K_0 \right),$$
26.

$$A^{(\mathbf{P})} = \rho^2 \left(\sigma_{01} - \sigma_0 \frac{\gamma_1}{\gamma_0} \right),$$
27.

$$\Pi^a = \rho^2 \frac{3R^2}{10} K_0.$$
28.

These expressions capture, in a continuum setting, the physics of stress generation by motor–filament interactions. Such effects were also discussed in the context of a discrete model in Reference 77. The signs of the coefficients in Equations 26–28 are set by the anisotropies of motor-mediated filament interactions. In particular, the balance between anisotropy of motor force (σ_{10}, σ_{01}) and anisotropy of motor friction (γ_1) is important. How the coefficients γ_1, σ_{10}, and σ_{01} are set remains an open question. Some specific cases can, however, be worked out from microscopic models. For instance, if one considers a molecular-scale motor with two identical heads, one finds that this motor would generate no active stress because $\sigma_1 = \gamma_1/\gamma_0\sigma_0$ by construction. One can argue further that adding a passive cross-link to the system allows γ_1/γ_0 to change without changing σ_1. Thus, such a motor can generate active stress, but to do so requires the presence of a passive cross-linker.

An analogous calculation provides expressions for the filament speed $\mathbf{v}_i$ and rotation rate $\dot{\mathbf{p}}_i$ in the lab frame:

$$\mathbf{v}_i - \mathbf{v} = \frac{\sigma_0}{\gamma_0}(\mathbf{p}_i - \mathbf{P}) + \mathcal{O}(L^2)$$
29.

and

$$\dot{\mathbf{p}}_i = (\mathcal{I} - \mathbf{p}_i\mathbf{p}_i) \cdot \left\{ \begin{array}{l} (\nabla \mathbf{v} + \frac{\sigma_0}{\gamma_0} \nabla \mathbf{P}) \cdot \mathbf{p}_i \\ + \frac{12}{\gamma_0 L^2 \rho^2} \mathcal{E} \cdot \mathbf{p}_i \\ + \frac{12}{\gamma_0 L^2} A^{(\mathbf{P})} \mathbf{P} \end{array} \right\},$$
30.

where $\mathcal{E}$ is the steric distortion field (9). We refer the reader to Reference 20 for additional detail.

Note that our discussion here largely ignores the fact that filaments in cytoskeletal networks are elastic and deformable. Of course whether this is important is a matter of filament length

scales and applied forces (short filaments are hard to bend relative to long ones). That said, filament deformability may have important consequences for the large-scale physics of cytoskeletal materials. In particular, it has been argued that the buckling or plucking of elastic filaments (78–80) can modify active stresses in cytoskeletal networks. In the context of microscopically based continuum theories, these effects remain unexplored.

4.4. The Sparsely Cross-Linked Regime of Cytoskeletal Networks

We now review theories of the sparsely cross-linked regime of cytoskeletal networks. We consider a cytoskeletal material to be sparsely cross-linked if $\ell^s \gg \ell^g$, so that the hydrodynamic (long-wave) limit is dominated by fluid-mediated interactions and the viscous transport of momentum though the gel is negligible (see **Figure 3**). Thus, these approaches proceed from Equation 4. Given a microscopic model of how the gel deforms in the fluid, these models proceed to calculate the active stresses $\boldsymbol{\Sigma}^a$, typically reflecting force dipoles acting on the solvent. Thus, $\Gamma\rho(\mathbf{v} - \mathbf{v}^s) \simeq \nabla \cdot \boldsymbol{\Sigma}^a$. This implies $\boldsymbol{\Sigma}^{\mathrm{tot}} = \boldsymbol{\Sigma}^s + \boldsymbol{\Sigma}^a$. The motion of the gel generally takes the form $\mathbf{v}^s - \mathbf{v} \propto \mathbf{P}$, which allows polar pieces of gel to swim through the solvent.

One such line of models devolves from the mechanics of swimming suspensions. To study the dynamics of suspensions of hydrodynamically interacting swimming microorganisms, Saintillan & Shelley (81, 82) developed a kinetic theory coupling a Smoluchowski equation for particle position and orientation to a forced Stokes equation (see also 22, 83, 84). At the particle level, free swimmers (which are force dipoles in the solvent) are treated as rod-like particles swimming in a locally linear flow, propelled by a prescribed active surface stress. The swimmer velocity, rotation rate, and entire surface stress can be calculated in terms of the background flow, with the background flow itself determined through solution of a forced Stokes equation. The forcing is through an extra stress found using Batchelor's adaptation (85), for dilute suspensions, of Kirkwood theory. In its simplest formulation, Saintillan & Shelley find the coupled Smoluchowski equation for the particle distribution function $\psi(\mathbf{x}, \mathbf{p}, t)$:

$$\partial_t \psi + \nabla_x \cdot (\dot{\mathbf{x}}\psi) + \nabla_p \cdot (\dot{\mathbf{p}}\psi) = 0, \text{ where } \dot{\mathbf{x}} = \mathbf{v}^s(\mathbf{x}) + U_0\mathbf{p} \text{ and } \dot{\mathbf{p}} = (\mathbf{I} - \mathbf{pp})\nabla\mathbf{v}^s(\mathbf{x})\mathbf{p}, \qquad 31.$$

where $\mathbf{p}$ is swimmer orientation and U_0 is its undisturbed speed, and the last expression is Jeffrey's equation (cf. Equations 29 and 30). The solvent velocity $\mathbf{v}^s$ is found through solution of a Stokes equation driven by an active dipolar stress $\boldsymbol{\Sigma}^a$:

$$- \nabla_x \Pi^s + \mu\Delta\mathbf{v}^s = -\nabla_x \cdot \boldsymbol{\Sigma}^a \text{ and } \nabla_x \cdot \mathbf{v}^s = 0, \text{ with } \boldsymbol{\Sigma}^a = \alpha_0\rho\mathcal{Q}. \qquad 32.$$

Here, α_0 is the so-called dipole strength whose sign reflects whether the swimmer force dipole is extensile ($\alpha_0 < 0$) or contractile ($\alpha_0 > 0$). This categorization depends upon the detailed placement of thrust and no-slip regions on the effective swimmer body. This theory predicts instabilities of both aligned suspensions (86, 87) and isotropic extensile suspensions when swimmers exceed a critical concentration (82, 87, 88). In later work (87), interparticle aligning torques and consequent stresses, based on Maier–Saupe theory (8), were introduced to capture sterically induced concentration effects (see 22 for a review).

Gao et al. (12, 89) adapted this approach to treating immersed assemblies of microtubules undergoing polarity sorting by multimeric motor complexes such as the engineered kinesin-1 complexes used in Reference 64. To do this, as the basic unit they considered nematically ordered local clusters of microtubules, say, with n of them pointing rightward and m pointing leftward [hence, $\mathbf{P} = (n - m)/(n + m)\hat{\mathbf{x}}$; see Reference 12, their figure 1]. It is assumed that every microtubule pair in the cluster is connected by active, plus-end directed cross-linkers moving at speed v_w on each

microtubule. The coupling between the antialigned populations induces a minus-end directed relative sliding for each. By using Stokesian slender-body theory (90) and assuming that the solvent drag thus calculated is the only force resisting microtubule motion, they calculated the velocities of the left- and rightward pointing microtubules to be $v_L = (2n/n + m)v_w$ and $v_R = -(2m/n + m)v_w$. This yields $v_R - v_L = -2v_w$. Slender-body theory again yields the forces each rod exerts upon the fluid, and hence the induced extra stress tensor arising from polarity sorting within the bundle can be calculated and is found to be proportional to $v_w mn/(m + n)\hat{\mathbf{x}}\hat{\mathbf{x}}$.

Thus, in a cluster with $m = n$, the two populations are pulled past each other with equal speed v_w while producing a maximal polarity-sorting stress. If most microtubules point rightward, so that $m \approx 0$, then $v_L \approx 2v_w$ and $v_R \approx 0$, and the polarity sorting extra stress is small (with a like statement if $n \approx 0$). That the microtubule speeds depend upon the polarity is a consequence of the micromechanical model wherein only solvent drag resists microtubule translocation.

Adapting this cluster picture to a more general setting in which the cluster also moves with the background fluid velocity, Gao et al. give the analogous result to Equations 31 and 32, where the microtubule flux and active stress tensor, induced by polarity sorting of antialigned microtubules (*aa*), are given by

$$\dot{\mathbf{x}} = \mathbf{v}^s(\mathbf{x}) + v_w(\mathbf{P} - \mathbf{p}), \text{ and } \mathbf{\Sigma}^{aa} = \alpha_{aa}\rho(\mathcal{Q} - \mathbf{PP}). \qquad 33.$$

These forms for $\dot{\mathbf{x}}$ and $\mathbf{\Sigma}^{aa}$ reproduce exactly the nematic cluster results above, and show the dependence–polarity sorting of the microtubule velocity upon the local polarity $\mathbf{P(x)}$.

This theory was further informed by detailed Brownian/Monte-Carlo simulations of nematic assemblies of rigid filaments interacting through multimeric kinesin-1 motors, thermal noise, and steric interactions. From these simulations were gleaned estimates of the activity coefficient α_{aa} giving that $\alpha_{aa} < 0$, i.e., that polarity-sorting dipolar stresses were extensile (12, 89). The stochastic simulations also showed the presence of an additional subdominant, active and extensile stress, having the form $\alpha_{pa}\rho(\mathcal{Q} + \mathbf{PP})$, arising from the relaxation of cross-link tethers of multimeric motors connecting polar-aligned (*pa*) microtubules (91). With this continuum model in hand, they analyzed and simulated the dynamics of a thin layer of active material at the interface between two fluids. Their analysis demonstrated the existence of a characteristic finite length scale of instability due to the external drag of the outer fluids and of orientational instabilities for aligned states. Their simulations of the full kinetic theory showed a nonlinear dynamics of fluid and material flows, and of nucleating/annihilating disclination defect pairs, with a structure qualitatively similar to that observed experimentally in Reference 64.

To make comparisons to the highly cross-linked regime, the total stress in the Gao et al. model has the form

$$\mathbf{\Sigma}^{\text{tot}} = \mathbf{\Sigma}^s + \mathbf{\Sigma}^a = -\Pi^s\mathcal{I} + \mu\left(\nabla\mathbf{v}^s + \nabla\mathbf{v}^{sT}\right) + (\alpha_{pa} + \alpha_{aa})\rho\mathcal{Q} + (\alpha_{pa} - \alpha_{aa})\rho\mathbf{PP} + \tilde{\mathbf{\Sigma}}^s, \qquad 34.$$

where $\tilde{\mathbf{\Sigma}}^s$ contains stresses arising from steric interactions (from Maier–Saupe theory) and particle rigidity (compare to Equation 11). Here, the microtubule flux in Equation 33 is of the same form as in the highly cross-linked case but with the solvent velocity rather than the material velocity $\mathbf{v}$ (14) (compare Equation 29). Unlike the stress in the highly cross-linked regime, the expression in Equation 34 does not depend upon $\nabla\mathbf{P}$. It is the relation between $\nabla\mathbf{P}$ and $\nabla\mathbf{v}$ revealed by Equation 24 that underlies the self-straining state of the highly cross-linked state (see **Figure 5**).

The cluster picture in Reference 12 can be generalized by allowing cluster–cluster interactions that can lead to additional stresses proportional to the gradient in the local polarity. Efforts along these lines were first made in References 76 and 92–94. There the key assumption is that pairs of filaments interact via sparse coupling of constant velocity motors. This theory also provided an initial understanding of the origin of contractile behaviors found in many early experiments of filament–motor mixtures.

5. SYNTHESIS AND OPEN CHALLENGES

Cytoskeletal networks are the drivers of basic biological functions like cell division and cell motility. The constituents of cytoskeletal networks also provide foundational examples in the field of active matter. In this review, we highlight the differences between the physics of highly cross-linked and sparsely cross-linked cytoskeletal networks. In highly cross-linked systems, the long-ranged transport of momentum is mediated through the cross-links themselves ($\ell^g \gg \ell^s$), whereas in sparsely cross-linked systems it is the solvent that plays that role ($\ell^s \gg \ell^g$) (see **Figure 3**).

This has important implications for the resulting material properties. In highly cross-linked materials, the same cross-linkers that generate the driving forces between filaments also generate the frictional coupling that keeps the networks coherent. Consequently, active stresses and the viscosity of the material are intimately linked. In particular, the polar active stress proportional to polarity gradients is linked to the viscosity tensor by Equation 23. For these materials, the viscous and polar stresses exactly balance when all filaments in the material move at the preferred motor velocity σ_0/γ_0 in the direction to which they point (14). Because χ^v and χ^a vary together, the properties of this state are not sensitive to protein concentrations. This self-straining state is not just a theoretical curiosity; it has been observed in vitro (14) and in spindles (17, 95).

In contrast, in the sparsely cross-linked regime the viscosity tensor χ^v of the material is largely set by the viscosity of the solvent in which filaments are suspended and is thus independent of concentrations and properties of the cross-linking molecules, whereas the values of active stresses depend on protein concentrations. This provides a possible diagnostic for differentiating highly cross-linked and sparsely cross-linked active materials by modulating cross-link concentrations. Furthermore, in the self-straining state of active materials filaments can move through the material at speeds that are independent of the local polar and nematic order (14), whereas in more sparsely cross-linked systems (12) the motion of filaments throughout the system depends on the local polarity.

A second striking difference between the highly cross-linked and sparsely cross-linked materials is the form of the other active stresses, $\mathcal{A}^{(Q)}$ and $\mathcal{A}^{(\mathbf{P})}$. It has long been known that contractile (or extensile) stresses can be generated only if motors act in a way that breaks the symmetry between extending and contracting single filament pairs. This could, for instance, be achieved by end-clustering or end-binding affinities of motor proteins (18, 93, 94). On top of that, the mathematics of the highly cross-linked regime require that $\sigma_1 \neq \gamma_1/\gamma_0\sigma_0$ (see Equations 26 and 27). This means that the anisotropy of friction (γ_1/γ_0) along filaments needs to be different from the anisotropy of motor drive (σ_1/σ_0) to generate active contractions. In practice, this can be achieved by either mixing several types of cross-links or creating a cross-link with two different motor heads (20). This prediction might shed insight into the well-known—but so far poorly understood—observation that in many actomyosin systems contractions only occur if a small amount of passive cross-linker is added to the system (96).

A third important difference between the highly and sparsely cross-linked regimes comes from the fact that the solvent is incompressible, whereas the network itself can be compacted by active processes. As a consequence, sparsely cross-linked theories predict incompressible material flow fields, whereas highly cross-linked theories can predict active bulk contraction. Thus, it is tempting to speculate that contractile systems like those in References 71 and 72 are highly cross-linked. In contrast, many classic active nematic experiments show no clear signs of compaction (42, 64, 67).

In Section 3, we sought to classify biological and experimental active matter systems as being either highly or sparsely cross-linked. We believe that many important systems, such as the cell cortex and many spindles, are highly cross-linked. For most systems, however, this assertion remains an educated guess rather than an experimental certainty. Given the increasing awareness

that the physics of active cytoskeletal networks can be drastically different for different numbers of cross-links, we hope that this review will serve to highlight the need for experiments that will answer this question more definitively.

Finally, we want to conclude by remarking that many active systems are likely to live in the intermediate regime between highly and sparsely cross-linked. One example is the microtubule asters studied in extract (63), which are probably highly cross-linked in their bulk but are more sparsely cross-linked near their boundaries. These structures are biologically important and revelatory of new physics in an intermediate cross-linking regime that is so far barely explored.

In summary, we firmly believe that the science of biologically active materials will benefit greatly by simply enumerating the number of cross-links active in the materials of interest. This enumeration will help identify important and distinct physical regimes and help make theories of quantitative and living systems engineerable.

DISCLOSURE STATEMENT

ACKNOWLEDGMENTS

LITERATURE CITED

1. Howard J. 2001. *Mechanics of Motor Proteins and the Cytoskeleton*. Sunderland, MA: Sinauer Assoc.
2. Alberts B, Johnson A, Lewis J, Raff M, Roberts K, Walter P. 2007. *Molecular Biology of the Cell*. New York: Garland Sci. 5th ed.
3. Foster PJ, Fürthauer S, Shelley MJ, Needleman DJ. 2019. *Curr. Opin. Cell Biol.* 56:109–14
4. Kruse K, Joanny JF, Jülicher F, Prost J, Sekimoto K. 2005. *Eur. Phys. J. E* 16(1):5–16
5. Fürthauer S, Strempel M, Grill S, Jülicher F. 2012. *Eur. Phys. J. E* 35:89
6. Jülicher F, Grill SW, Salbreux G. 2018. *Rep. Prog. Phys.* 81(7):076601
7. Naganathan SR, Fürthauer S, Rodriguez J, Fievet BT, Jülicher F, et al. 2018. *eLife* 7:e37677
8. Doi M, Edwards SF. 1988. *The Theory of Polymer Dynamics*, Vol. 73. Oxford, UK: Oxford Univ. Press
9. de Gennes PG, Prost J. 1995. *The Physics of Liquid Crystals*. Oxford, UK: Clarendon Press. 2nd ed.
10. Liverpool TB, Marchetti MC. 2003. *Phys. Rev. Lett.* 90(13):138102
11. Aranson IS, Tsimring LS. 2005. *Phys. Rev. E* 71(5):050901
12. Gao T, Blackwell R, Glaser MA, Betterton MD, Shelley MJ. 2015. *Phys. Rev. Lett.* 114(4):048101
13. Broedersz CP, MacKintosh FC. 2014. *Rev. Mod. Phys.* 86(3):995–1036
14. Fürthauer S, Lemma B, Foster PJ, Ems-McClung SC, Yu CH, et al. 2019. *Nat. Phys.* 15(12):1295–300
15. Mitchison T. 1989. *J. Cell Biol.* 109(2):637–52
16. Yang G, Cameron LA, Maddox PS, Salmon ED, Danuser G. 2008. *J. Cell Biol.* 182(4):631–39
17. Dalton BA, Oriola D, Decker F, Jülicher F, Brugués J. 2021. bioRxiv 2021.01.15.426844. **https://doi.org/10.1101/2021.01.15.426844**
18. Kruse K, Jülicher F. 2000. *Phys. Rev. Lett.* 85(8):1778–81
19. Kruse K, Jülicher F. 2003. *Phys. Rev. E* 67(5):051913
20. Fürthauer S, Needleman DJ, Shelley MJ. 2021. *N. J. Phys.* 23(1):013012
21. Marchetti M, Joanny JF, Ramaswamy S, Liverpool TB, Prost J, et al. 2013. *Rev. Mod. Phys.* 85(3):1143–89
22. Saintillan D, Shelley MJ. 2013. *C. R. Phys.* 14(6):497–517

23. Maryshev I, Marenduzzo D, Goryachev AB, Morozov A. 2018. *Phys. Rev. E* 97(2):022412
24. Janson ME, Loughlin R, Loïodice I, Fu C, Brunner D, et al. 2007. *Cell* 128(2):357–68
25. Head D, Briels W, Gompper G. 2014. *Phys. Rev. E* 89:032705
26. Popov K, Komianos J, Papoian GA. 2016. *PLOS Comput. Biol.* 12(4):e1004877
27. Freedman SL, Banerjee S, Hocky GM, Dinner AR. 2017. *Biophys. J.* 113(2):448–60
28. Collinet C, Lecuit T. 2021. *Nat. Rev. Mol. Cell Biol.* 22:245–65
29. Redemann S, Baumgart J, Lindow N, Shelley M, Nazockdast E, et al. 2017. *Nat. Commun.* 8:15288
30. Pollard TD. 2016. *Cold Spring Harb. Perspect. Biol.* 8(8):a018226
31. Alfaro-Aco R, Petry S. 2015. *J. Biol. Chem.* 290(28):17154–62
32. Luby-Phelps K. 1999. *Int. Rev. Cytol.* 192:189–221
33. Garzon-Coral C, Fantana HA, Howard J. 2016. *Science* 352(6289):1124–27
34. Salbreux G, Charras G, Paluch E. 2012. *Trends Cell Biol.* 22(10):536–45
35. Mayer M, Depken M, Bois JS, Jülicher F, Grill SW. 2010. *Nature* 467(7315):617–21
36. Gross P, Kumar KV, Goehring NW, Bois JS, Hoege C, et al. 2019. *Nat. Phys.* 15(3):293–300
37. Callan-Jones A, Ruprecht V, Wieser S, Heisenberg CP, Voituriez R. 2016. *Phys. Rev. Lett.* 116(2):028102
38. Turlier H, Audoly B, Prost J, Joanny JF. 2014. *Biophys. J.* 106(1):114–23
39. Chugh P, Clark AG, Smith MB, Cassani DA, Dierkes K, et al. 2017. *Nat. Cell Biol.* 19(6):689–97
40. Naganathan SR, Fürthauer S, Nishikawa M, Jülicher F, Grill SW. 2014. *eLife* 3:e04165
41. Li D, Shao L, Chen B-C, Zhang X, Zhang M, et al. 2015. *Science* 349(6251):aab3500
42. Wu K-T, Hishamunda JB, Chen DTN, DeCamp SJ, Chang Y-W, et al. 2017. *Science* 355(6331):eaal1979
43. Fritzsche M, Erlenkämper C, Moeendarbary E, Charras G, Kruse K. 2016. *Sci. Adv.* 2(4):e1501337
44. Wu JQ, Pollard TD. 2005. *Science* 310(5746):310–14
45. Brugués J, Nuzzo V, Mazur E, Needleman DJ. 2012. *Cell* 149(3):554–64
46. Brugués J, Needleman D. 2014. *PNAS* 111(52):18496–500
47. Petry S, Pugieux C, Nédélec FJ, Vale RD. 2011. *PNAS* 108(35):14473–78
48. Petry S, Groen AC, Ishihara K, Mitchison TJ, Vale RD. 2013. *Cell* 152(4):768–77
49. Oh D, Yu CH, Needleman DJ. 2016. *PNAS* 113(31):8729–34
50. Kaye B, Stiehl O, Foster PJ, Shelley MJ, Needleman DJ, Fürthauer S. 2018. *N. J. Phys.* 20(5):055012
51. Decker F, Oriola D, Dalton B, Brugués J. 2018. *eLife* 7:e31149
52. Thawani A, Kadzik RS, Petry S. 2018. *Nat. Cell Biol.* 20(5):575–85
53. Thawani A, Stone HA, Shaevitz JW, Petry S. 2019. *eLife* 8:e43890
54. Redemann S, Fürthauer S, Shelley M, Müller-Reichert T. 2019. *Curr. Opin. Struct. Biol.* 58:269–77
55. Redemann S, Lantzsch I, Lindow N, Prohaska S, Srayko M, Müller-Reichert T. 2018. *Curr. Biol.* 28(18):2991–97
56. Lantzsch I, Yu CH, Yazdhkasti H, Lindow N, Szentgyoergyi E, et al. 2021. 10:e58903
57. Pavin N, Laan L, Ma R, Dogterom M, Jülicher F. 2012. *N. J. Phys.* 14(10):105025
58. Nazockdast E, Rahimian A, Needleman D, Shelley M. 2017. *Mol. Biol. Cell* 28(23):3261–70
59. Farhadifar R, Yu CH, Fabig G, Wu HY, Stein DB, et al. 2020. *eLife* 9:e55877
60. Sulerud T, Sami AB, Li G, Kloxin A, Oakey J, Gatlin J. 2020. *Mol. Biol. Cell* 31(25):2791–802
61. Meaders JL, Burgess DR. 2020. *Cells* 9(2):505
62. Xie J, Minc N. 2020. *Front. Cell Dev. Biol.* 8:69
63. Pelletier JF, Field CM, Fürthauer S, Sonnett M, Mitchison TJ. 2020. *eLife* 9:e60047
64. Sanchez T, Chen DT, DeCamp SJ, Heymann M, Dogic Z. 2012. *Nature* 491(7424):431–34
65. Keber F, Loiseau E, Sanchez T, DeCamp S, Giomi L, et al. 2014. *Science* 345:1135–39
66. Opathalage A, Norton MM, Juniper MP, Langeslay B, Aghvami SA, et al. 2019. *PNAS* 116(11):4788–97
67. Chandrakar P, Varghese M, Aghvami SA, Baskaran A, Dogic Z, Duclos G. 2020. *Phys. Rev. Lett.* 125(25):257801
68. Čopar S, Aplinc J, Kos Ž, Žumer S, Ravnik M. 2019. *Phys. Rev. X* 9(3):031051
69. Duclos G, Adkins R, Banerjee D, Peterson MS, Varghese M, et al. 2020. *Science* 367(6482):1120–24
70. Banerjee S, Gardel ML, Schwarz US. 2020. *Annu. Rev. Condens. Matter Phys.* 11:421–39
71. Foster PJ, Fürthauer S, Shelley MJ, Needleman DJ. 2015. *eLife* 4:e10837
72. Foster PJ, Yan W, Fürthauer S, Shelley MJ, Needleman DJ. 2017. *N. J. Phys.* 19(12):125011

73. Needleman D, Dogic Z. 2017. *Nat. Rev. Mater.* 2:17048
74. Chaikin PM, Lubensky TC. 1995. *Principles of Condensed Matter Physics* Cambridge, UK: Cambridge Univ. Press
75. Kruse K, Zumdieck A, Jülicher F. 2003. *Europhys. Lett.* 64(5):716
76. Liverpool TB, Marchetti MC. 2006. *Phys. Rev. Lett.* 97(26):268101
77. Belmonte JM, Leptin M, Nédélec F. 2017. *Mol. Syst. Biol.* 13(9):941
78. Ronceray P, Broedersz CP, Lenz M. 2016. *PNAS* 113(11):2827–32
79. Lenz M, Thoresen T, Gardel ML, Dinner AR. 2012. *Phys. Rev. Lett.* 108(23):238107
80. Lenz M. 2014. *Phys. Rev. X* 4:041002
81. Saintillan D, Shelley MJ. 2008. *Phys. Rev. Lett.* 100(17):178103
82. Saintillan D, Shelley MJ. 2008. *Phys. Fluids* 20(12):123304
83. Subramanian G, Koch DL. 2009. *J. Fluid Mech.* 632:359–400
84. Baskaran A, Marchetti MC. 2009. *PNAS* 106(37):15567–72
85. Batchelor G. 1970. *J. Fluid Mech.* 44:419–40
86. Simha RA, Ramaswamy S. 2002. *Phys. Rev. Lett.* 89(5):058101
87. Ezhilan B, Shelley MJ, Saintillan D. 2013. *Phys. Fluids* 25(7):070607
88. Hohenegger C, Shelley MJ. 2010. *Phys. Rev. E* 81:046311
89. Gao T, Blackwell R, Glaser MA, Betterton MD, Shelley MJ. 2015. *Phys. Rev. E* 92:062709
90. Keller JB, Rubinow SI. 1976. *J. Fluid Mech.* 75(4):705–14
91. Blackwell R, Sweezy-Schindler O, Baldwin C, Hough LE, Glaser MA, Betterton M. 2016. *Soft Matter* 12(10):2676–87
92. Liverpool TB, Marchetti MC. 2005. *Europhys. Lett.* 69(5):846–52
93. Ahmadi A, Marchetti MC, Liverpool TB. 2006. *Phys. Rev. E* 74(6):061913
94. Liverpool TB, Marchetti MC. 2008. In *Cell Motility*, ed. P Lentz, pp. 177–206. New York: Springer
95. Yang G, Cameron L, Maddox P, Salmon E, Danuser G. 2008. *J. Cell Biol.* 182:631–39
96. Ennomani H, Letort G, Guérin C, Martiel JL, Cao W, et al. 2016. *Curr. Biol.* 26(5):616–26